Erklärung zur Abschlussarbeit gemäß § 22 Abs. 7 APB TU Darmstadt

Hiermit erkläre ich, Jan Kröger, dass ich die vorliegende Arbeit gemäß § 22 Abs. 7 APB der TU Darmstadt selbstständig, ohne Hilfe Dritter und nur mit den angegebenen Quellen und Hilfsmitteln angefertigt habe. Ich habe mit Ausnahme der zitierten Literatur und anderer in der Arbeit genannter Quellen keine fremden Hilfsmittel benutzt. Die von mir bei der Anfertigung dieser wissenschaftlichen Arbeit wörtlich oder inhaltlich benutzte Literatur und alle anderen Quellen habe ich im Text deutlich gekennzeichnet und gesondert aufgeführt. Dies gilt auch für Quellen oder Hilfsmittel aus dem Internet.

Diese Arbeit hat in gleicher oder ähnlicher Form noch keiner Prüfungsbehörde vorgelegen.

Mir ist bekannt, dass im Falle eines Plagiats (§ 38 Abs. 2 APB) ein Täuschungsversuch vorliegt, der dazu führt, dass die Arbeit mit 5,0 bewertet und damit ein Prüfungsversuch verbraucht wird. Abschlussarbeiten dürfen nur einmal wiederholt werden.

Bei einer Thesis des Fachbereichs Architektur entspricht die eingereichte elektronische Fassung dem vorgestellten Modell und den vorgelegten Plänen.

Darmstadt, 12. Oktober 2023

J. Kröger

Contents

Todo list

1 Introduction

Many everyday phenomena that we observe are, contrary to expectations, not yet fully understood. This does not mean that they are not utilized in a variety of technical devices. In the case of wetting, we encounter many different things in everyday life, such as a drop on a window pane that seems to slide down randomly, or the sleeve of a sweater that seems to soak up water when washing hands.

Nature has a head start in this effect and has produced creatures that can walk on water because they take advantage of the water's surface tension. The flora also uses surface tension, whether it's trees that wouldn't reach the size we know without the capillary effect, or the lotus flower, which, with its water-repellent (hydrophobic) surface, ensures that water rolls off and takes dirt with it in the process.

Porous media, through their use in oxygenators, became lifesavers during the Corona pandemic by reoxygenating blood. The potential applications and necessities of this phenomenon could be demonstrated with many more examples. This work aims to describe the dynamics of capillary rise through simulations. A porous medium can be simplified as a collection of many small tubes. Insights from these small tubes can then be extrapolated to determine the behavior of the porous medium. Therefore, experiments with both porous media and individual capillaries are of great interest to understand how the rise in the capillary is designed. Simulations of these processes are also increasingly being carried out, as they have the advantage of fixing certain relevant material properties to examine their influence, or to look into areas that would not be possible with a conventional experimental setup.

In this work, the rise of a liquid column (water) in a capillary is investigated. Specifically, for a two-phase system, the area around the interface in the water phase is examined, and how dissipative processes in this region influence the rise of the water column. Possible phase changes (evaporation, boiling, condensation, etc.) are not taken into account. An isothermal and isobaric system is also assumed. All fluids treated are Newtonian, and the flow can be assumed to be Poiseuille flow. Furthermore, newly implemented boundary conditions of the used solver, which are supposed to better represent the behavior of the contact line and contact angle, will also be checked.

This work will first discuss important findings in the description of capillary rise, the contact line, and the simulation of such problems with phase field methods in Chapter **??**. This is followed by an overview of the important influencing factors of wetting and

their influence on the topics discussed in Chapter 2. Chapter 3 provides an introduction to the phase field method and how it is implemented to simulate such problems. Chapter 5 shows that the solver used has already shown in many other simulations that it produces correct results and is applicable to these problems. Validation of the geometries used here is not possible due to their size, as they have a radius of 3 nm. It is not currently known that there are experiments that provide reliable results with a constant cross-section and such small radii. Subsequently, Chapter 4 describes the setup of the simulations with descriptions of the geometry, material properties used, and solver settings. Finally, the results are discussed in Chapter , and an outlook for upcoming investigations is given in Chapter .

ADD CHAPTER

ADD CHAPTER

The solver used here is `phaseFieldFoam`, which is an extension of the open-source environment `OpenFOAM-extend`. The version used of `OpenFOAM-extend` is 5.0, and the version of the solver is still in development. The further development and maintenance of the solver are carried out through a cooperation between KIT (Karlsruhe Institute of Technology) and TU Darmstadt, especially by Dr.-Ing. Xuan Cai and Dr.-Ing. Holger Marschall. The simulations for this research were conducted on the Lichtenberg high-performance computer of the TU Darmstadt.

Here a introduction, but probably only after the most is done and the layout of the thesis is set.

The dynamics of a rising fluid in the capillary is the subject of many processes. In nature, for example, trees would not be able to grow as high as they do without the capillary effect, and in technology many processes with a porous medium exist. Porous media can be simplified as many small tubes through which a fluid travels. Therefore, this process has long been of great interest in science and yet there are many uncertainties in the description of the dynamics.

The Lucas Washburn equation, introduced in 1921 [**lucas_ueber_1918**, **washburn_dynamics_1921**], attempts to describe the height of the propagating fluid column as a function of time. This equation is sufficiently accurate for many applications.

However, due to the assumptions made in the derivation of the equation, it is clear that it cannot be applied to every problem. Therefore, there are many approaches to adapt this equation to problems and simply maintain the behaviour of the equation.

It is shown, that the Lucas Washburn equation has its problems in early stages of the imbibition[**bosanquet_lv_1923**, **quere_inertial_1997**], due to the undefined behaviour for $t = 0$ and neglecting the inertia of the fluid.

check if quere1997 is also a source. Probably talked about that. Maybe even Washburn talked about that?

The early stages of the imbibition process is yet to be understood and in this work we show how the different forces are acting on the meniscus for small time steps with a simulation of the such a problem. This simulations are done with the open source framework of foam extend, which is a fork of open foam. Here the department of mathmatics of the TU Darmstadt and the KIT developed a solver for a phase field approach.

rework this regment.

The developed solver phaseFieldFoam is maintained and developed by the department of MMA at the Tu darmstadt and ... KIT. It is using the Phase field approach to solve the Navier Stokes Equations (NSE).

In this work, first the attempts to describe the imbibition of a fluid in a capillay, especially for the early stages and small capillaies are discussed. Followed by the work, which has been done to simulate such problems with the phase field approach. Important interrelationships and derivations of the process of wetting is discussed, again followed by the equivalent numerical relations. How the simulations are setup and the results are in the chapers and .

ref chapter

ref chapter

ref to both chapters

chapter

chapter

Lucas needed to prewet the tube to get the results he predicted

In this work

2 Wetting Theory

The wetting theory describes the interaction of fluids with solid surfaces. Many processes in nature, as well as in technology, are affected by this phenomenon. In this work, the focus is on the wetting properties in capillaries, which are often used as a simplification for understanding porous media or in other processes, such as the fact that trees would not be as tall as they are today without this effect.

First, an overview of some types of wetting is presented , and the concepts of contact angle and contact line are introduced. Subsequently, the surface tension and its role in wetting are discussed. Since this work considers the dynamic rise of a water column in a capillary, the dynamic contact angle is also examined in Chapter , followed by a description of the capillary effect and its significance for the rise of a fluid in a capillary.

ref

ref

ref chapter

ref

rework

2.1 Surface Tension

Surface tension plays a significant role in the wetting of surfaces or in capillary rise. Therefore, it is essential to first clarify what surface tension is. In general, surface tension is a proportionality constant that depends on temperature, pressure, and the phases involved but is independent of the surface [7]. The interface separates the phases and can be interpreted differently. On a molecular level, molecules attract each other (cohesion). The interaction between two phases is called adhesion. In the case of the interaction between a liquid and a solid, adhesion can usually be neglected. In Figure 2.1, a water droplet surrounded by air is illustrated on the left. The black outer line thus represents the interface between the droplet and the air. If one now magnifies the transition area down to the molecular level (red area), one obtains the schematic representation on the right side. The blue circles are simplified representations of the water molecules, and the gray ones represent the surrounding air. Here, it is evident how, at the interface, the water molecules are no longer surrounded only by other water molecules, which is energetically unfavorable. However, since the system strives to transition into an energetically favorable state, it attempts to minimize the number of molecules lying at the interface [7].

possibly ref to corresponding chapters here.

To increase the surface area, molecules must be transported to the surface, and energy must be supplied to the system. Therefore, surface tension is also interpreted as the

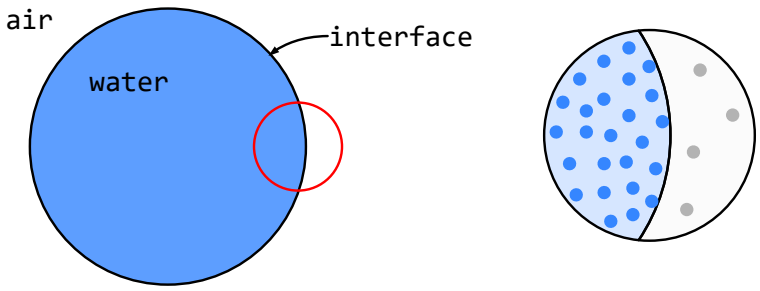

Figure 2.1: Schematic of interacting molecules in a liquid droplet and its interaction with a vapor

necessary energy required to carry a molecule to the surface.

$$dE = \sigma \cdot dA \tag{2.1}$$

with dE as the supplied energy and dA as the change in surface area.

2.2 Wetting Phenomenon

Despite the fact that the wetting of droplets is not considered in this work, it is appropriate to describe the fundamentals of wetting using this example. The concepts are the same, and many initial studies are based on this example.

In the case where the system is in equilibrium, Young [47] derived an equation relating surface tensions to the contact angle:

$$\sigma_{\mathrm{LV}} \cdot \cos\theta_{\mathrm{e}} = \sigma_{\mathrm{SV}} - \sigma_{\mathrm{SL}} \tag{2.2}$$

Where σ_{LV} is the surface tension between the liquid and the gas, σ_{SV} is from the solid to the gas, and σ_{SL} is between the solid and the liquid (see Figure 2.2). If $(\sigma_{\mathrm{SV}} > \sigma_{\mathrm{SL}})$ holds true, a contact angle less than $90°$ follows; otherwise, $90° \leq \theta_{\mathrm{e}} < 180°$. In the case where $\sigma_{\mathrm{SV}} = \sigma_{\mathrm{SL}} + \sigma_{\mathrm{LV}}$, complete wetting of the surface occurs [7].

When a droplet impacts a solid surface, different states can arise depending on the fluid-solid combination. At the point where the interface of the two fluids (droplet and surrounding fluid) meets the solid surface, the contact line is formed (see 2.2; red line). Depending on the fluid-fluid-solid combination, a contact angle θ_{e} is established, where the suffix e stands for equilibrium. In the case of complete wetting, the fluid spreads over the entire surface (see Figure 2.3 a)). This effect, however, is challenging to reproduce as it can be hindered by surface irregularities [7]. As seen in Figure 2.3(b-d)), states where a droplet forms on the surface are further subdivided. For a contact angle $\theta_{\mathrm{e}} < 90°$, it is

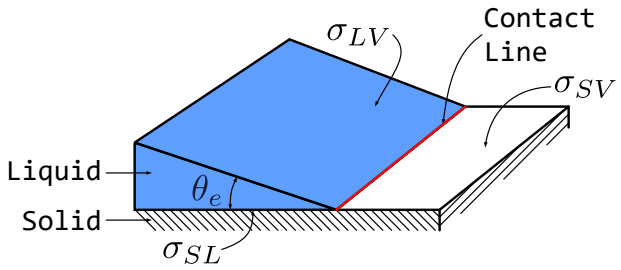

Figure 2.2: Three Phase Contact Line

termed hydrophilic (see 2.3b)), for $\theta_e > 90°$ it's hydrophobic (see 2.3c)), and for a contact angle $\theta_e > 120°$, it's superhydrophobic surfaces (see 2.3d)). Developing superhydrophobic surfaces is also challenging. To curve the surface of the liquid, a pressure difference must

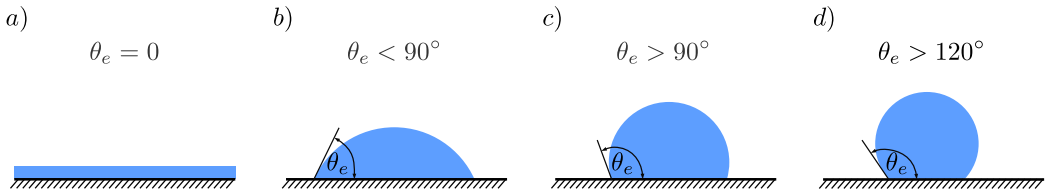

Figure 2.3: Wetting of a surface

exist. In the case of a sphere, Young and Laplace developed a relationship for the pressure difference in terms of the surface tension and radius as:

$$P_\mathrm{i} - P_\mathrm{o} = \Delta P = \frac{2\sigma}{R} \tag{2.3}$$

With ΔP being the pressure difference at the interface, P_i as the pressure inside the droplet, P_o the ambient pressure, and R as the radius of the sphere. For a derivation, refer to [7].

2.2.1 Dynamic Weting

So far, only states have been considered that observe systems in equilibrium. Typically, however, the contact line is in motion. When the contact line is moving, the contact angle (dynamic contact angle θ_D) differs from that in the equilibrium state [4]. To describe the dynamics of the contact line, the dynamic contact angle, the relative speed of the contact line, and the equilibrium contact angle are required [34, 4, 14, 26, 42]. However, describing the contact line is challenging due to the fact that the microscopic level affects the macroscopic level.

In Figure 2.4, various views of the contact line are illustrated. The red circle in *a)* points to the area considered in the picture next to it and can be understood as a magnifying glass. If we enlarge the area in *a)*, we see the interpretation of the contact line from the perspective of the hydrodynamic theory, with a microscopic contact angle θ_{m} and the dynamic contact angle θ_{D} (Figure 2.4 *b)*). Focusing again on the contact line, we see the interpretation of the molecular kinetic theory (Figure 2.4 *c)*). The illustrated points are intended to represent molecules in a simplified form.

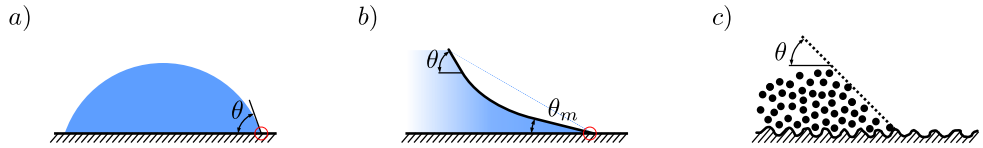

Figure 2.4: Hydrodynamic and Molecular Kinetic description of the Contact angle. Figure b) corresponds to the area circled in red in a), and c) to the area from image b).

Hydrodynamic Theory The hydrodynamic approach solves the physics of the flow using the Navier-Stokes equations but encounters a singularity at the contact line when a sticking condition is applied [26]. To address this issue, either the sticking condition near the wall was relaxed or the solution was truncated at the molecular level [4]. In both cases, a small capillary number is assumed, which means that far from the contact line, the interface assumes its equilibrium shape.

Voinov [42] derived a description of the contact line for a spreading droplet depending on the capillary number. A generalized version was developed by Cox [14] with some correction terms [11, 4]. Thus, the dynamic contact angle for $\theta_{\mathrm{D}} \leq 3/4\pi$ is given by

$$\theta_D^3 - \theta_m^3 = 9Ca \ln\left(\frac{L}{L_m}\right) = 9\frac{\mu u}{\sigma} \ln\left(\frac{L}{L_m}\right) \tag{2.4}$$

With L as the macroscopic path length and L_{m} as the microscopic path length. Assuming that the interface assumes its equilibrium shape far away, $\theta_{\mathrm{m}} = \theta_{\mathrm{e}}$. However, Voinov himself already pointed out that θ_{m} could also depend on the speed [42, 4, 31].

Molecular Kinetic Theory The Molecular Kinetic Model describes the movement of the contact line with a statistical description of the molecular movement at the contact line [3]. In contrast to the hydrodynamic model, the molecular processes at the contact line influence those of the larger scales. In this view, the molecules at the contact line jump back and forth to adsorption sites on the solid substrate. The speed of the contact line is determined by multiplying the difference between the forward and backward jumps by a

jump distance λ. This results in the description

$$u = 2\lambda\kappa_0 \sinh\left(\frac{\sigma\left(\cos\theta_\mathrm{e} - \cos\theta_\mathrm{D}\right)}{2nk_\mathrm{B}T}\right). \tag{2.5}$$

Where n is the number of adsorption sites per unit area, k_0 is a characteristic frequency, k_B is the Boltzmann constant, and T is the temperature. If the system is in equilibrium, the forward and backward jumping is balanced, and the contact line comes to a standstill [10, 4]. However, a problem with this view is that this model is more qualitative and computationally intensive [34].

2.2.2 Capillary Rise

A capillary is a very thin tube in which, due to surface effects, a liquid rises or falls without external force. In 2.5, a capillary with an already risen liquid column is shown. The well-known surface tensions are also marked at their respective locations, as well as the essential geometric parameters, such as diameter ($2R$) or height of the resulting meniscus z. The resulting contact angle after reaching equilibrium, θ_e, is also shown. The system in this representation is also subject to gravitational forces.

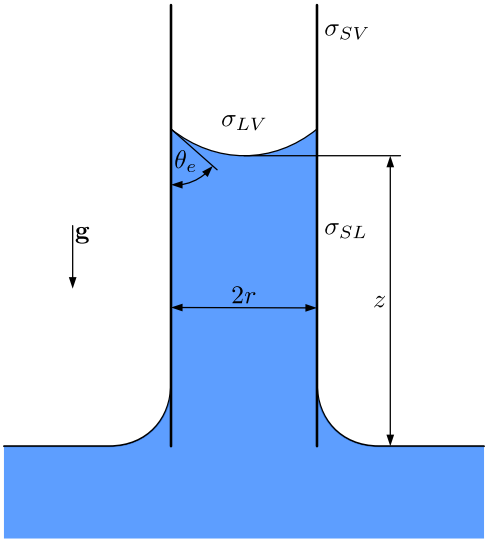

Figure 2.5: Schematic representation of a capillary in a liquid after it has penetrated the capillary.

In this work, such a system is used. However, further conditions apply. It is assumed that the system is isobaric, isothermal, and the liquid is Newtonian. Furthermore, it is assumed that while the water column rises in the capillary, a Poiseuille flow is present and no phase

change occurs. It is also assumed that the viscosity of the gas phase is negligible. With these assumptions and boundary conditions, the Newtonian dynamics in a capillary can be described as a balance between the inertial forces and the sum of the capillary forces, viscous forces, and hydrostatic forces [20]:

$$\frac{d}{dt}M(z,\dot{z}) = F_{\mathrm{w}} - F_{\eta} - F_{\mathrm{g}} \tag{2.6}$$

With $M(z,\dot{z}) = \pi r^2 \rho z \dot{z}$ as the moment, $F_{\mathrm{g}} = \pi r^2 \rho g z$ as the gravitational force, and F_{η} as the viscous resistance, which results from the assumption of the average velocity and the existing Poiseuille flow to $F_{\eta} = 8\pi\eta z\dot{z}$. With $\dot{z}$ as the average velocity. The capillary forces result from the previous description of the surface tension and the change in the surface of the meniscus with a change in the current height:

$$F_{\mathrm{w}} = \sigma\frac{dA}{dz} = \sigma 2\pi r \tag{2.7}$$

The surface tension σ here is the increase in surface energy due to the wetting of the solid wall of the capillary. Thus, $\sigma = \sigma_{\mathrm{SV}} - \sigma_{\mathrm{SL}}$. This description is already known from the Young equation (2.2). Thus, after inserting for the capillary forces:

$$F_W = \sigma_{\mathrm{LV}} \cdot \cos\theta_{\mathrm{e}} 2\pi r. \tag{2.8}$$

Thus, for equation 2.6 after insertion [20]:

$$\pi r^2 \rho \frac{d}{dt}(z\dot{z}) = \sigma_{\mathrm{LV}} \cdot \cos\theta_{\mathrm{e}} 2\pi r - 8\pi\eta z\dot{z} - \pi r^2 \rho g z. \tag{2.9}$$

Early descriptions by Bell and Cameron [2] did not describe the rise dynamics based on equation 2.9. They developed the rise dynamics from experiments according to:

$$z(t)^n = K \cdot t. \tag{2.10}$$

Both n and K are temperature-dependent constants. In 1918, Lucas [32] and in 1921, Washburn [43] derived the Lucas Washburn equation by neglecting the inertial and gravitational terms:

$$z(t) = \sqrt{\frac{r\sigma\cos\theta_{\mathrm{e}}}{2\eta}t} \tag{2.11}$$

With this, they independently developed an equation with which the capillary rise can be described based on material values and measurements. Therefore, it gained popularity

over the years. Due to the neglect of individual terms and simplifications in the system, however, this equation is not always precise for several reasons. Washburn himself pointed out that to meet the prediction of the equation, he had to set up the experiments in such a way that the capillary was prewetted. Therefore, adjustments to this equation were made for various problems [17, 24, 8, 21, 20, 16, 33]. Wu et al. [45] examined several models and compared them with experiments. In these, however, it is always assumed that the height of the meniscus increases according to $z(t) \sim \sqrt{t}$ as well.

Bosanquet [6] hinted in his 1923 paper that equation 2.11 would lead to unphysical behavior for $t \to 0$ and also developed an equation that retained this problem but now also included inertia and can give a better prediction of the rise for early times of imbibition, but also fails for small capillary [13].

Siegel [39] studied the rise behavior under microgravity and found a linear growth. However, he did not reach the Lucas-Washburn regime. Zhmud et al. [51] also pointed out the problems for times near 0 from equation 2.11 and described a quadratic relationship for the times when the fluid is drawn into the capillary, followed by the known Lucas-Washburn regime.

Dreyer et al. [19] studied parallel plates under microgravity and divided the rise of the meniscus into three regions. Starting with a quadratic growth, followed by a linear region, and finally the Lucas-Washburn growth. Quéré [36] showed a linear growth at the beginning by assuming that in this case only inertia plays a role. Stange [40] confirmed the three regions of Dreyer et al. [19] and derived dimensionless equations to develop transition times.

Fries et al. [22] divided the growth area into areas where different forces act. In the beginning, inertia dominates, followed by a transition area where the viscous forces take over until they finally dominate. They also developed dimensionless times at which the transition takes place.

At the point where the viscous friction and the effects of inertia or dynamic contact angle are equal, Quéré [36] and Fries et al. [22] defined the characteristic penetration length:

$$l_\mathrm{c} \propto r\sqrt{\frac{r\rho\sigma}{\mu^2}} \tag{2.12}$$

Dellanoy et al. [16] focused on early times and studied viscous fluids, confirming the influence of pre-wetting the capillary, as already mentioned by Washburn [43]. They also showed a deviation from the Lucas-Washburn regime at early times. They attributed this deviation to local viscous dissipation in the wedge region, rather than a global dissipation as assumed by Lucas and Washburn. Regarding the dynamic contact angle, they showed that the characteristic penetration length (cf. Equation 2.12) is calculated as:

$$l_\mathrm{c} \propto r \ln\left(\frac{r}{l_\mathrm{m}}\right) \tag{2.13}$$

With l_m being the microscopic length that compensates for the singularity of the contact line [14]. They further assumed that once l_c is reached, the transition to the Lucas-Washburn regime occurs.

Ruiz-Gutiérrez et al. [37] contradicted this statement in their work, showing that this transition takes longer. They argue that the effects of inertia and dynamic contact angle do not decay exponentially.

To account for this, they expanded Equation 2.9 for problems with a moving interface by introducing:

$$f(\dot{z}) \equiv \frac{\cos\theta_{\mathrm{m}} - \cos\theta_D(\dot{z})}{\cos\theta_{\mathrm{m}}} \tag{2.14}$$

With the assumption that for $u > 0$ from Equation 2.4, $\theta_{\mathrm{D}} > \theta_{\mathrm{m}}$ holds true, this function disappears for $\theta_{\mathrm{D}} \to \theta_{\mathrm{m}}$.

Now, considering the moving system, Equation 2.9 for the case studied in this work becomes:

$$\pi r^2 \rho z \frac{du}{dt} = 2\pi r\sigma\cos\theta_{\mathrm{m}} + \pi r^2\rho g z - 8\pi\sigma z\dot{z} - 2\pi r\sigma\cos\theta_{\mathrm{m}} f \tag{2.15}$$

With the first two terms as driving forces and the last two as resistance forces. The last term has been added and acts as a correction for the fact that the dynamic contact angle does not correspond to the macroscopic contact angle.

Subsequently, dimensionless quantities were introduced, and four cases were defined. Two each with a large and small Laplace number, or a large and small ratio of length scales. With the quantities used in this work, case three from Ruiz-Gutiérrez et al. [37] should apply. They predict that the quadratic regime will not occur, and the rise will begin with a linear region, eventually transitioning to the Lucas-Washburn regime.

maybe use this eq instead of shorted one?

$$\pi r^2 \rho l \frac{\mathrm{d}u}{\mathrm{d}t} = 2\pi r\gamma\cos\theta_{\mathrm{a}} + \pi r^2\rho g h - 8\pi\mu l u - \frac{3}{2}\pi r^2\rho u^2 - 2\pi r\gamma\cos\theta_{\mathrm{a}} f \tag{2.16}$$

2.3 Simulating the Wetting Processes

Simulating a two-phase flow can be achieved through several methods. Common approaches include the `Volume-of-Fluid` and the `Level-Set` methods. Both methods use a sharp interface and are based on the Hydrodynamic Theory from Chapter 2.2.1. Moreover, they are *interface capturing* methods, so they don't require recalculating the computational grid over the simulation period. Other methods that follow the interface (*interface tracking*) are also possible. One of the major drawbacks of these methods is that the moving contact line, when using the adhesion condition, depends on models [11].

Additionally, calculating the surface tension can pose a challenge. This requires computing the curvature of the surface, which can lead to relatively high numerical errors [29, 23].

The Lattice-Boltzmann Method uses collision models to describe fluid behavior. Surface tensions can be considered through modifications. There are approaches that are promising and some are comparable to the phase-field method. However, one of the biggest challenges is the limitation of density or viscosity ratios. In this work, the fluids have significantly different densities with a ratio of 1000. According to [12], the Lattice-Boltzmann Method is limited to ratios of $\mathcal{O}(10)$ and can lead to instabilities otherwise.

Another frequently used method is `Molecular Dynamic` simulations. Since individual molecules are simulated in this case, this method is only applicable to geometrically and temporally small problems without driving computational costs too high. Therefore, `Molecular Dynamic` simulations are often used for comparison or to study only small problems ([15, 31, 33, 17]).

The method used in this work is the `phase-field` method. This method models two or even multi-phase flow through the system's free energy. A more detailed description of this method and the simulations already carried out is provided in Chapter 3.

Elaborate or maybe move the entire section to phase field? Or perhaps case setup with a reasoning why phase field?

3 Phase Field Method

The phase field method, rooted in system thermodynamics, offers a solution for an interface with a finite thickness, an idea originating from van der Waals in 1893 [41]. This method models the free energy of the system and can derive a phase field method for interfacial dynamics. It offers several advantages, such as mass conservation, contact line motion, and adherence to thermodynamic laws. In contrast to the hydrodynamic theory, the contact line moves through interfacial diffusion. However, there are concerns about its validity in modeling macroscopic contact line motion, especially regarding the sharp-interface limit. Despite these concerns, meaningful results have been predicted on the macro scale that align with hydrodynamic theory and experimental observations[50, 48, 10].

Phase field simulations for macroscopic wetting typically rely on the Cahn-Hilliard equations. For slow wetting phenomena, the phase field theory has been both analytically [28] and numerically [48, 50] proven to capture such wetting physics. However, for rapid spreading of water drops, the assumption of local equilibrium may not hold. Some studies have introduced a boundary condition for wetting far from equilibrium, introducing a parameter that controls the relaxation towards equilibrium . This parameter has been interpreted in various ways, from a local friction adjacent to the contact line to a relaxation parameter at the contact line[49][11].

Phase Field Theory Die Phasenfeld theorie verwendet Ansätze beider Modelle unter verwendung der Beschreibung der freien Energie des Systems.

ref chapter Phase-Field

Daher ist es auch notwendig für die Phasenfeldmethode sowohl hydrodynamische Ansätze als auch Ansätze der Molekular Kinetik Theorie zu verwenden [4, 11].

vof and level setzt difference interface tracking and capituring?

Free energy system

einleitende Worte

Wie bereits in Kapitel 2.1 beshcrieben, gibt es unterschiedliche Möglichkeiten das Interface zu beschreiben. Hydrodynamische Modelle beschreiben das Interface so, dass am Übergang der Phasen die Stoffwerte springen. Ein Diffuses Interface hingegen, beschreibt die größen anders.

picture of interfaces

3.1 Phase Field Method in the Spirit of Cahn and Hillard

The phase field method traces back to the idea of van der Waals [41], who described the interface between two immiscible fluids from a thermodynamic perspective. In this description, the material properties transition continuously within a thin layer. Within this layer, both phases coexist.

Building on this, Cahn and Hillard [30] derived a description of the free energy in a volume with non-uniform composition as a function of an order parameter C for time-dependent problems. In its closed form, it reads

$$\partial C + \mathbf{u} \cdot \nabla C = \nabla \cdot (\kappa \nabla \phi(C)) \,. \tag{3.1}$$

Here, $\mathbf{u}$ is the velocity, κ is a diffusion coefficient, often referred to as mobility, and ϕ is a chemical potential. The order parameter indicates which phase is present and ranges between -1 and 1 for a two-phase system. The mobility can be related to the Péclet number, which represents the ratio of advective to diffusive fluxes with a characteristic path length (L_{char}) and velocity (u_{char}), as well as a characteristic chemical potential [9, 25].

The chemical potential is defined as the derivative of the Helmholtz free energy with respect to the order parameter [30]. In the system under consideration, the total free energy consists of the mixing energy and the interfacial density energy. According to [50], the system's free energy is influenced by two factors; defined over the volume Ω and the surface $\partial\Omega$

check!!!

$$F(C, \nabla C) = \int_\Omega f_{\text{mix}}(C, \nabla C) d\mathbf{x} + \int_{\partial\Omega} f_{\text{w}}(C) dS \tag{3.2}$$

Here, the first integral represents the mixing energy density f_{mix}, and the second represents the wall energy f_w.

3.1.1 Mixing Energy

Cahn and Hillard defined a mixing energy (f_{mix}) that depends on the order parameter and its gradient:

$$F(C, \nabla C) = \int_\Omega f_{\text{mix}}(C, \nabla C) d\mathbf{x} = \int_\Omega \left(\frac{\lambda}{\epsilon^2} \Psi(C) + \frac{\lambda}{2} |\nabla C|^2 \right) d\mathbf{x} \tag{3.3}$$

check if right function

The integration of the mixing energy over the domain yields the Helmholtz free energy of the fluid system and consists of two terms. The first term separates the phases from each other, while the second term mixes the phases. λ is a mixing energy parameter, ϵ a measure for the thickness of the interface, and Ψ a potential. The potential is chosen according to Ginzburg and Landau so that it has two minima at positions -1 and 1 and is

check if already mentioned

cite

given by

$$\Psi(C) = \frac{1}{4}\left(C^2 - 1\right)^2. \tag{3.4}$$

This leads to the following representation for the chemical potential

$$\Phi(C) := \frac{\partial F(C)}{\partial C} = \frac{\lambda}{\epsilon^2}\Psi'(C) - \lambda\nabla^2 C. \tag{3.5}$$

3.1.2 Diffusive Interface

The Cahn-Hillard model can describe systems with multiple fluids. However, only a binary fluid system is considered in this work. Figure 3.1 shows the contact line of a

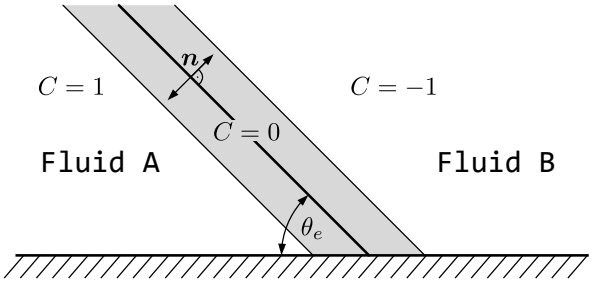

Figure 3.1: Schematic representation of a diffusive interface

diffusive interface. The gray area is the transition area of the order parameter and thus the material quantities. Within this area, both fluids coexist with their respective densities and viscosities. In the equilibrium state, the profile of C normal to the interface can be determined by minimizing the free energy (Equation 3.5) [9]. This then leads to a description of the order parameter normal to the interface with

$$C(n) = \tanh\left(\frac{n}{\sqrt{2}\epsilon}\right). \tag{3.6}$$

Here, n is the normal to the interface. In equilibrium, the thickness of the diffuse interface remains constant in a range of $3/\sqrt{2}\epsilon$ and for the order parameter $-0.9 \leq C \leq 0.9$. Also in the case of equilibrium, the surface tension equals the integral of the free energy density at the interface, from which a description for the surface tension can be derived [28].

$$\sigma = \int_{-\infty}^{\infty} \lambda \left(\frac{dC}{dn}\right)^2 = \frac{2\sqrt{2}}{3}\frac{\lambda}{\epsilon} \tag{3.7}$$

3.1.3 Wall Energy

Jaqcmin [27] postulated a wall energy of the form

$$F_{\mathrm{w}} = \int \sigma g(C) dA, \tag{3.8}$$

where the wall energy is now only a function dependent on the fluid composition directly at the wall. The resulting natural phase field boundary condition with local thermal equilibrium is given by

$$\lambda \frac{\partial C}{\partial n_{\partial\Omega}} + f'_{\mathrm{w}}(C) = 0. \tag{3.9}$$

With $n_{\partial\Omega}$ as the normal direction on the wall (cf. 3.1). The normal direction to the interface can be described with the wall normal and wall tangential direction on the wall.

$$n = n_{\partial\Omega} \cos(\theta_{\mathrm{e}}) + \tau_{\partial\Omega} \sin(\theta_{\mathrm{e}}). \tag{3.10}$$

Subsequently, for the first term from Equation 3.9 with Equations 3.10, 3.6, and 3.7, the following can be established

$$\lambda \frac{\partial C}{\partial n_{\partial\Omega}} = \underbrace{\frac{3}{4}\sigma \left(1 - C^2\right) \cos\theta_{\mathrm{e}}}_{=: -f'_{\mathrm{w}}(C)}. \tag{3.11}$$

From this, a function for the wall energy density can be derived after integration [28][25].

$$f_{\mathrm{w}}(C) = -\sigma \cos\theta_{\mathrm{e}} \frac{C(3 - C^2)}{4} + \frac{\sigma_{S_L} + \sigma_{S_V}}{2} \tag{3.12}$$

When only one of the phases is present, this equation only returns the respective surface tension. However, Yue et al. [49] point out that this description of wall energy for equilibrium contact angles close to $0°$ or $180°$ is difficult to reproduce, and the model is not capable of handling precursor films. With equations 3.9 and 3.12 and the definition of zero flux through the wall, the wetting boundary condition can be described as

$$\frac{\partial C}{\partial n_{\partial\Omega}} = \frac{\cos\theta_{\mathrm{e}}}{\sqrt{2}\epsilon}(1 - C^2). \tag{3.13}$$

Non Equilibrium Boundary Condition In aller Regel wird die Gleichgewichts Randbedingung verwendet (Gleichung 3.9) und vernachlässigen dabei ungleichgewichte nahe der Wand. Jacqmin [28] entwickelte und Yue et al. [49] bzw. Qian et al. [35] studierten eine generalisierte Variante von Gleichung 3.9.

$$\frac{\partial C}{\partial t} + \mathbf{u}_{\mathrm{w}} \cdot \nabla C = -\Gamma_{\mathrm{w}} \underbrace{\left(\lambda \frac{\partial C}{\partial n_{\partial\Omega}} + f'_{\mathrm{w}(C)}\right)}_{=: \phi_{\mathrm{w}}} \tag{3.14}$$

Mit Γ_w als einer neu eingeführten Konstante, genannt *wall relxation parameter*. Die Geschwindigkeit der Wand ist durch $\mathbf{u}_w$ gegeben. Nach Qian et al. [35] folgt für $\Gamma_w \to 0$ und $\kappa \to 0$ das sharp interface limit mit dominanter advektion. Für den gegenteiligen Fall folgt eine dominante Diffusion. Der wall relxation parameter ist ein paramter ist für die Simulation eine Einstellgröße und sollte as phänomenologischer parameter verstanden werden. Dieser parameter hängt sowohl vom Fluid system als auch von der Fluid wand Kombination ab[28].

3.2 Cahn-Hillard Navier Stokes Equations

The coupled Cahn-Hillard Navier Stokes equations are given by

$$\partial_t C + \nabla \cdot (C\mathbf{u}) = -\nabla \cdot \mathbf{J} \tag{3.15}$$

$$\nabla \cdot \mathbf{u} = 0 \tag{3.16}$$

$$\partial_t(\rho\mathbf{u}) + \nabla \cdot (\rho\mathbf{u}\mathbf{u}) = -\nabla\tilde{p} + \nabla\tau - \nabla \cdot (\mathbf{u}\mathbf{J}) - \phi\nabla C + \mathbf{f}_b \tag{3.17}$$

Wherein, $\tilde{p}$ is a modified pressure that arises from the Korteweg tensor to account for capillarity and is defined as

$$\tilde{p} = p + \frac{f_{\text{mix}}}{2}. \tag{3.18}$$

Assuming a Newtonian fluid, $\tau = 2\mu \text{dev}\mathbf{D}$ with $\mathbf{D} = 1/2[\nabla\mathbf{u} + (\nabla\mathbf{u})^T]$ as the deformation tensor. Furthermore, the density ρ and viscosity μ are volumetrically averaged with

$$\rho = \frac{1+C}{2}\rho_1 + \frac{1+C}{2}\rho_2. \tag{3.19}$$

Here, the suffixes 1 and 2 are markers for the respective phases. The viscosity is calculated analogously. The term $-\nabla \cdot (\mathbf{u}\mathbf{J})$ is necessary to ensure thermal consistency [18]. $\mathbf{J}$ is the phase-field flux and, according to Landau and Lifshitz , $\mathbf{J} = -\kappa\nabla\phi$ and therefore the phase-field system is driven by the gradient of the local chemical potential.

cite

4 Case Setup

Die Geometrie und einige Stoffeigenschaften sind durch die in 2 definierten vereinfachungen und Annahmen bereits vorgegeben. Im folgen wird zu beginn die Geometrie der Kapillare vorgestellt, gefolgt von den Materialeigenschaften und verwendeter Randbedingunen. Da mehrere Untersuchungen unternommen wurden, erfolgt in Kapitel eine Übersicht über die durchgeführten Simulationen und dessen Initialiserung.

ref

Wie bereits in Kapitel 1 geschrieben, erfolgen die Simulationen mit dem solver `phaseFieldFoam`. Dieser wurde bereits mehrfach Validiert, worauf in Kapitel 5 genauer eingegangen wird.

4.1 Geometry and Discretization

Die Geometrie der Kapillare wird so angenommen, dass sie wie in Abbildung 4.1 zu sehen, ein Reservoir mit Wasser hat, welches durch Oberflächeneffekte in die Kapillare strömt. Durch die Annahme, dass sich ein Teil des Wassers bereits in der Kapillare befindet, wird in der Simulieren Geometrie lediglich die Randbedingung so gesetzt, dass das Wasser in diesem Reservoir nachströmen kann und das Reservoir nicht mit modelliert und diskretisiert werden muss. Die Dimensionen der Kapillare ergeben sich daraus, dass die Simulation der Kapillare perspektivisch auch mit experimenten verglichen werden soll. Daher wurden auch weitere, komplexere Geometrien simuliert, die jedoch nicht Teil dieser Arbeit sind. Wie zu erkennen, handelt es sich um eine Kapillare mit lediglich $6nm$ Durchmesser. Eine Simulation so kleiner Kapillare wurde soweit bekannt bisher nicht mit der Phasenfeld methode Simuliert.

Wie bereits im Bild angedeutet wird nicht die gesamte Kapillare simuliert, sondern lediglich ein segment der Kapillare, *wedge* genannt. Dabei wird angenommen, dass die Strömung in der Kapillare achsensymmetrisch ist, was die Simulation dahingehend stark vereinfacht, dass zur Diskretisierung weniger Elemente benötigt werden, da in diesem Fall nur ein $5°$ großes Segment der Kapillare simuliert wird. Eine notwendige Bedingung zur Simulation der Wedge ist es, dass diese nur ein Element in radialer Richtung haben darf. Die Diskretisierung der Geometrie wurde so gewählt, dass die Elemente eine Kantenlänge von $0.2nm$ haben. Zur erstellung der `blockMeshDict`-datei, wurde ein python skript erstellt, welches anhand des Kapillardurchmessers und länge eine Datei mit den in Abbildung 4.1 dargestellten Benennungen der Oberflächen erstellt.

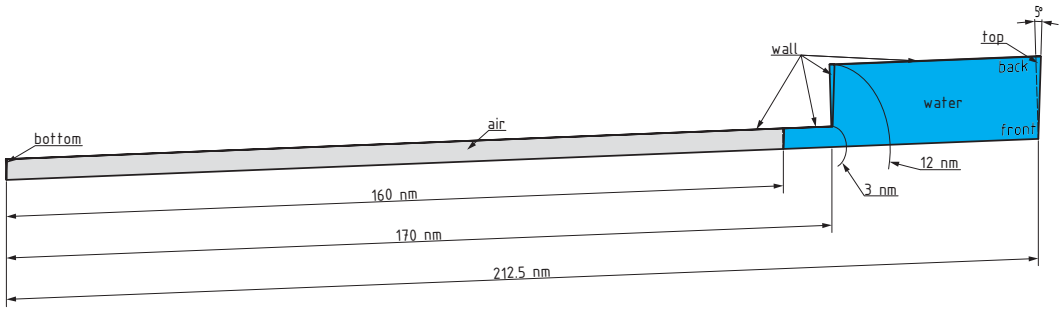

Figure 4.1: Schematic of used Capillary

4.2 Randbedingunen

In Abbildung 4.1 sind neben der Geometrie auch die Flächen, die mit Randbedingungen versehen wurden benannt. Die Flächen `front` und `back` sind sich gegenüberliegende Flächen der Wedge und müssen dementsprechende Ranbedinungen erhalten. Die `wall` Flächen sind nicht durchdringbare Oberflächen und `top`, bzw. `bottom` Oberflächen durch die ein Fluss zugelassen wird. Die wesentlichen Randbedingunen an der Wand sind in Tabelle 4.1 aufgelistet.

Table 4.1: relevant boundary conditions wall

Parameter	Value
orderparameter C	`equilibriumPhaseContactAngle`
equilibrium contact angle θ_e	$15°$, $45°$, $75°$
chemisches Potential ϕ	`zeroGradient`
velocity $\mathbf{u}$	$\mathbf{u}_w = 0$
pressure p	`fixedFluxPressure`

Für den Ordnungsparameter C wird die Gleichgewichtsrandbedingung angenommen und der Gleichgewichtskontaktwinkel für jede der drei Simulationen mit dieser Geometrie mit $15°$, $45°$ bzw. $75°$ angegeben. Für weitere Simulationen wurde neben der genannten Gleichgewichtsbedingung `equilibriumPhaseContactAngle`, auch angenommen, dass ein ungleichgewicht nach 3.1.3 herrscht. Dazu muss für die Simulationen die Randbedingung zu `outOfEquilibriumPhaseContactAngle` geändert und ein Wert für Γ_w angegeben werden. Der Gradient des chemischen potentials an der Wand wird als null gesetzt, genauso wie die Geschwindigkeit der Wand. Die Ranbedingung für den Druck wird mit `fixedFluxPressure` so gewählt, dass der Druckgradient so angepasst wird, das der Massenfluss am Rand mit der vorgegebenen Geschwindigkeit an der Wand übereinstimmt. Am ein, bzw. Auslass der Kapillare gilt ebenfalls eine `zeroGradient` Randbedingungn und ein Druck von 0 Pa.

4.3 Materialeigenschaften

Für die Simulation werden unter anderem Wasser und Luft bei $25°$ Celsius als Medium angenommen. Damit folgen die in Tabelle 4.2 dargestellten Materialeigenschaften. Die

Table 4.2: Physical properties

fluid	density $\frac{kg}{m^3}$	kinematic viscosity $\frac{m^2}{s}$
water	1000	$1.00E-06$
air	1	$1.00E-05$

Oberflächenspannung für ein Wasser-Luft interface für $25°$ Celsius ist mit $0.072N/m$ gegeben. The interface thickness ϵ was chosen to be approximately $1.7nm$ [1], corresponding to the physical interface thickness.

4.4 Simulationsparameter

The mobility (κ) is a factor in the phase-field simulation that is difficult to determine. Jacqmin [27] suggested an asymptotic behavior for κ of

$$\kappa = \mathcal{O}(\epsilon^{\delta}) \tag{4.1}$$

and showed that $1 \leq \delta < 2$. Leider gibt es für die Mobility bisher keine konkrete Berechnungsmethode. Daher wurden mehrere Simulationen durchgeführt, um einen Wert zu finden. Das Gleiche gilt auch für den Wandrelaxationsfaktor Γ_{w}. Die tatsache, dass diese parameter phänomenologischer natur sind, macht es schwierig sie vorherzusagen und es gibt lediglich empfehlungen. For this work, a value of $\kappa = 1.6 \times 10^{-18}$ was used. Für den Wand relaxationsfaktor Γ_{w} wurde ein wert von $\kappa = 5 \times 10^{12}$ verwendet. CHECK

Durch anfängliche Probleme im Postprocessing wurde die Simulaiton nicht mit einer Adaptiven Netz verfeinerung durchgeführt. Die Simulation wurde mit planarem Interface initialisiert und für den Ordnungsparametermit hilfe der `funkySetFields` Methode ein interface profil nach Gleichung 3.6 initialisiert.

Die viskositätsmodell der Simulation wird mit der `blended`-Methode durchgeführt. Dabei werden die Modelle `arithmetic` und `harmonic` über einen blending-factor gemischt.

4.5 Auswertungsmethoden

Zur Auswertung der Simulation wurde unter anderem die Anwendung `paraview` verwendet. Alle bilder der Simulation wurden damit erzeugt. Die Auswertung und darstellung

abgeleiteter oder berechneter Größen in Diagrammen wurden hingegen mit der python bibliothek `Matplotlib` erzeugt. Dazu wurde ein skript erstellt, das die Ergebnisse der function objects sammelt und gegebenenfalls Berechnungen damit vornimmt.

Mit hilfe von *function objects* können während der laufenden Simulation daten erfasst werden. `phaseFieldFoam` liefert einige funktionen zum auslesen der Simulation mit, die auch hier verwendet werden. Diese Müssen in der `controlDict` datei eingebunden und konfiguriert werden.

Zur analyse der wirkenden viskosen Kräfte im der Wassersäule, benötigen wir die gesamte viskose dissipationskraft in jener Wassersäule. Diese erhalten wir, wenn die divergenz des viskosen stress tensors τ aus Gleichung 3.17 über das Gebiet integrieren

$$\mathrm{F}_{\mathrm{visc}}^{\mathrm{total}} = \int_{\Omega} \mathrm{f}_{\mathrm{visc}}\mathrm{total} dV = \int_{\Omega} \nabla \cdot \tau dV. \tag{4.2}$$

5 Validation

The `phaseFieldFoam`- Solver

Da solche Simulationen für so kleine Geometrien jedoch noch soweit bekannt bisher noch nicht mit einer Phasenfeld Methode durchgeführt wurden,

- Moradi2021 Laplace Test

Der Solver `phaseFieldFoam` wurde bereits mehrfach für unterschiedliche Probleme validiert. Auch Simulationen mit einer Wedge wurden in [25] mit Adaptiver Netzverfeinerung durchgeführt. Simulationen von Kapillaren oder auch parallelen Platten wurden in Hagg [23], bzw. von Cai et al. [9] durchgeführt. Samkhaniani et al. [38] simulierte einen springenden Tropfen auf einer hydrophoben Oberfläche. Viele weitere Interessante und wichtige Simulationen und Validierungen wurden mit `phaseFieldFoam` durchgeführt [5, 46, 44, 1], dessen einzelne Nennung den Rahmen dieser Arbeit sprengen würde. Da der solver bereits an vielen Stellen validiert wurde, wird in dieser Arbeit lediglich ein Laplace-Test durchgeführt. Dabei kann mit Gleichung 2.3 die Druckdifferenz bei einem sich einstellenden Radius des Interfaces der Simulation berechnet und mit dem Theoretischen wert Verglichen werden. Für diesen Vergleich muss der Radius des Interfaces in der Simulation bekannt sein. Um diesen zu erhalten, kann unter der Annahme, dass der Mittelpunkt des Kreises auf der Rotationsachse liegt, der Radius mit

$$r_{\mathrm{S}} = \frac{R^2}{2h} + \frac{h}{2} \tag{5.1}$$

berechnet werden.

In Abbildung 5.1 ist die Geometrie der Kapillare mit den relevanten Größen dargestellt. Die Punkte P_{R}, bzw. P_{A} sind die Schnittpunkte des Interfaces mit der Kapillarwand und der Rotationsachse. Sind diese Punkte bekannt, kann die höhe h des sphärenabschnitts berechnet werden und damit dann auch der Radius der sphäre r_{S} mit dem bereits bekannten Kapiilarradius R. Die gestrichelte Linie soll dabei verdeutlichen, dass der Radius der sphäre nicht dem der Kapillare entsprechen muss.

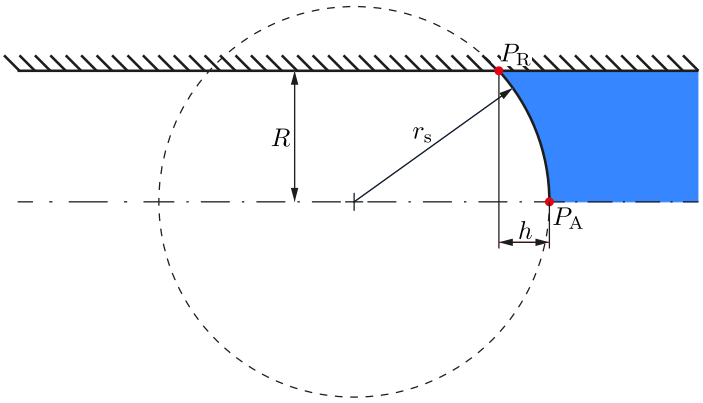

Figure 5.1: Schematic of capillary with relevant dimension for calculation of radius

6 Results

The Position of the meniskus was exported with paraview in the decomposed state. The position was then extracted with a python script.Probe data was preprocessed as well and several computations for eval of simulations. Plots were generated with matplotlib?; Start of real results with an overview when what where. Maybe work with normalized data?

Wie in Kapitel 2.2.2 gezeigt, ist der Kapillare Aufstieg bis heute nicht verstanden. Ziel dieser Arbeit ist es daher

Wie bereits beschrieben soll der Übergang vom linearen Anstieg der höhe einer Wassersäule in einer Kapillare hin zum Lucas Washburn Regime Untersucht werden. Weiter wurde beschrieben wie Delanoy et al. [16] oder Ruiz et al. [37] das Wachstum beschrieben. Zum Vergleich damit werden zunächst die Zeitpunkte oder Längen anhand ihrer vorhersagen berechnet und anschließend verglichen. Zunächst aber ein direkter Vergleich mit der Lucas-Washburn Gleichung. Delanoy et al. [16] oder Ruiz et al. [37] haben eigene Ansätze gefunden, um den Übergang zwischen den beiden Wachstumsregionen zu beschreiben.

Im folgenden werden die Ergebnisse der Simulationen diskutiert und versucht eine Beschreibung für den Übergang der vorgestellten Wachstumsregionen des Kapillaren Aufstiegs zu finden. Um mögliche einflüsse durch den Kontaktwinkel berücksichtigen zu können wurden die Simulationen mit drei unterschiedlichen Kontaktwinkeln durchgeführt. Bei den verwendeten Dimensionen der Kapillare und der Flüssigkeiten, ist zu erwarten, dass der Einfluss der Gravitation vernachlässigbar ist, was auch in gesondert durchgeführten Simulationen gezeigt werden konnte, jedoch aufgrund der geringen aussagekraft eines Vergleichs mit Simulationen ohne Gravitation nicht weiter betrachtet wird. Damit wird jedoch auch klar, dass eine der besprochenen von Lucas und Washburn angenommen Vereinfachnungen für diesen Fall nicht gelten und eine Abweichung der vorhersage mit Gleichung 2.11 darauf zurückzuführen ist, dass ein Gleichgewicht zwischen Kapillarkraft und viskosem drag nicht ausreicht, um den Kapillaren Aufstieg in frühen imbibitionsstadien zu beschreiben.

Abbildung 6.1 zeigt einen direkten vergleich der Simulationsergebnisse mit der Lucas-Washburn Gleichung (rote linie). Darin wurde in 6.1 (a) linear skalliert und in 6.1 (b) logarithmisch. In der logarithmischen Darstellung werden die Unterschiede deutlich sichtbar. Zu Beginn ist die Steigung der Simulationen größer als die der vorhersage, bis

describe as in actual figure later

sie sich schließlich annähern. Das lässt darauf schließen, dass der Kapillare Aufstieg erst nach einiger Zeit dem bekannten Lucas Washburn Wachstum folgt. Dies

Wie ebenfalls bereits beschrieben sagt die Lucas-Washburn Gleichung ein Wachstum von $z(t) \sim \sqrt{t}$ vorher.

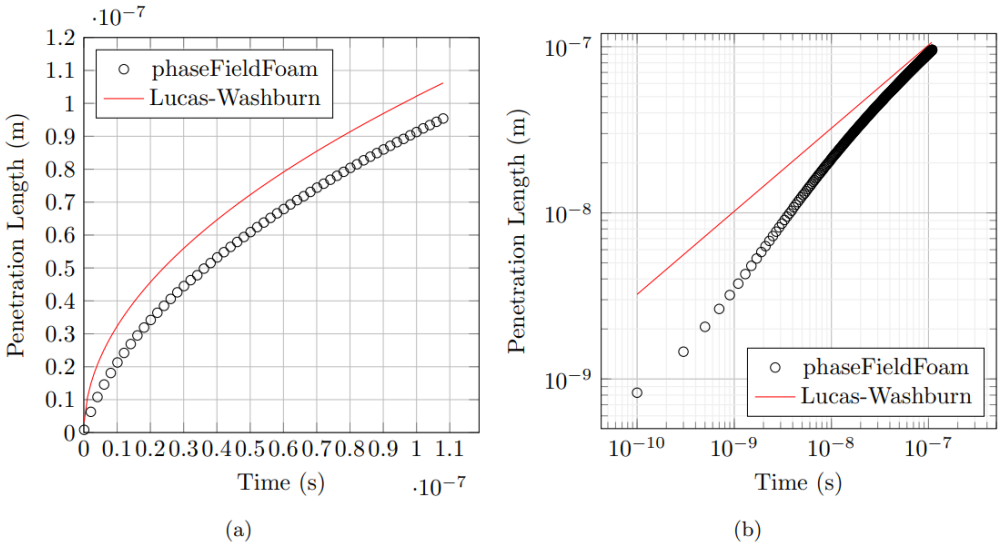

Figure 6.1: Vergleich des von Lucas-Washburn vorhergesagten Wachstums mit den Ergenissen von `phaseFieldFoam`

7 Outlook

- complex geometry
- temperature dependent capillary rise?
- surfactants and capillary rise?
- more fluids with other viscosisties
- in depth reseach of gamma value and possible dependence of mesh resolution

Bibliography

[1] Milad Bagheri et al. “Interfacial Relaxation – Crucial for Phase-Field Methods to Capture Low to High Energy Drop-Film Impacts”. In: *International Journal of Heat and Fluid Flow* 94 (Apr. 2022), p. 108943. ISSN: 0142727X. DOI: 10.1016/j.ijheatfluidflow.2022.108943. URL: https://linkinghub.elsevier.com/retrieve/pii/S0142727X22000182 (visited on 10/10/2023).

[2] J. M. Bell and F. K. Cameron. “The Flow of Liquids through Capillary Spaces”. In: *The Journal of Physical Chemistry* 10.8 (Nov. 1, 1906), pp. 658–674. ISSN: 0092-7325, 1541-5740. DOI: 10.1021/j150080a005. URL: https://pubs.acs.org/doi/abs/10.1021/j150080a005 (visited on 10/05/2023).

[3] T.D Blake and J.M Haynes. “Kinetics of Displacement”. In: *Journal of Colloid and Interface Science* 30.3 (July 1969), pp. 421–423. ISSN: 00219797. DOI: 10.1016/0021-9797(69)90411-1. URL: https://linkinghub.elsevier.com/retrieve/pii/0021979769904111 (visited on 10/05/2023).

[4] Terence D. Blake. “The Physics of Moving Wetting Lines”. In: *Journal of Colloid and Interface Science* 299.1 (July 2006), pp. 1–13. ISSN: 00219797. DOI: 10.1016/j.jcis.2006.03.051. URL: https://linkinghub.elsevier.com/retrieve/pii/S0021979706002463 (visited on 10/05/2023).

[5] Francisco Bodziony, Martin Wörner, and Holger Marschall. “The Stressful Way of Droplets along Single-Fiber Strands: A Computational Analysis”. In: *Physics of Fluids* 35.1 (Jan. 1, 2023), p. 012110. ISSN: 1070-6631, 1089-7666. DOI: 10.1063/5.0131032. URL: https://pubs.aip.org/pof/article/35/1/012110/2866965/The-stressful-way-of-droplets-along-single-fiber (visited on 10/05/2023).

[6] C.H. Bosanquet. “LV. *On the Flow of Liquids into Capillary Tubes*”. In: *The London, Edinburgh, and Dublin Philosophical Magazine and Journal of Science* 45.267 (Mar. 1923), pp. 525–531. ISSN: 1941-5982, 1941-5990. DOI: 10.1080/14786442308634144. URL: https://www.tandfonline.com/doi/full/10.1080/14786442308634144 (visited on 10/05/2023).

[7] Hans-Jürgen Butt, Karlheinz Graf, and Michael Kappl. *Physics and Chemistry of Interfaces*.

[8] Jianchao Cai et al. “Lucas–Washburn Equation-Based Modeling of Capillary-Driven Flow in Porous Systems”. In: *Langmuir* 37.5 (Feb. 9, 2021), pp. 1623–1636. ISSN: 0743-7463, 1520-5827. DOI: 10.1021/acs.langmuir.0c03134. URL: https://pubs.acs.org/doi/10.1021/acs.langmuir.0c03134 (visited on 10/05/2023).

[9] Xuan Cai et al. “Numerical Simulation of Wetting Phenomena with a Phase-Field Method Using OpenFOAM®”. In: *Chemical Engineering & Technology* 38.11 (Nov. 2015), pp. 1985–1992. ISSN: 0930-7516, 1521-4125. DOI: 10.1002/ceat.201500089. URL: https://onlinelibrary.wiley.com/doi/10.1002/ceat.201500089 (visited on 10/05/2023).

[10] A. Carlson, M. Do-Quang, and G. Amberg. “Dissipation in Rapid Dynamic Wetting”. In: *Journal of Fluid Mechanics* 682 (Sept. 10, 2011), pp. 213–240. ISSN: 0022-1120, 1469-7645. DOI: 10.1017/jfm.2011.211. URL: https://www.cambridge.org/core/product/identifier/S0022112011002114/type/journal_article (visited on 10/05/2023).

[11] Andreas Carlson. “Capillarity and Dynamic Wetting”. KTH Royal Institute of Technology, 2012.

[12] Li Chen et al. “A Critical Review of the Pseudopotential Multiphase Lattice Boltzmann Model: Methods and Applications”. In: *International Journal of Heat and Mass Transfer* 76 (Sept. 2014), pp. 210–236. ISSN: 00179310. DOI: 10.1016/j.ijheatmasstransfer.2014.04.032. URL: https://linkinghub.elsevier.com/retrieve/pii/S0017931014003378 (visited on 10/10/2023).

[13] Qu Chen and Jianping Zhou. “Investigating the Validity of the Bosanquet Equation for Predicting the Self-Diffusivities of Fluids inside Nanotubes Using Equilibrium Molecular Dynamics Simulations”. In: *AIP Advances* 13.2 (Feb. 1, 2023), p. 025338. ISSN: 2158-3226. DOI: 10.1063/5.0137310. URL: https://pubs.aip.org/adv/article/13/2/025338/2877685/Investigating-the-validity-of-the-Bosanquet (visited on 10/05/2023).

[14] R. G. Cox. “The Dynamics of the Spreading of Liquids on a Solid Surface. Part 1. Viscous Flow”. In: *Journal of Fluid Mechanics* 168 (-1 July 1986), p. 169. ISSN: 0022-1120, 1469-7645. DOI: 10.1017/S0022112086000332. URL: http://www.journals.cambridge.org/abstract_S0022112086000332 (visited on 10/05/2023).

[15] Deeptayan Datta et al. “Early-Stage Liquid Infiltration in Nanoconfinements”. In: *Langmuir* 39.9 (Mar. 7, 2023), pp. 3301–3311. ISSN: 0743-7463, 1520-5827. DOI: 10.1021/acs.langmuir.2c03154. URL: https://pubs.acs.org/doi/10.1021/acs.langmuir.2c03154 (visited on 10/05/2023).

[16] Joachim Delannoy et al. “The Dual Role of Viscosity in Capillary Rise”. In: *Soft Matter* 15.13 (2019), pp. 2757–2761. ISSN: 1744-683X, 1744-6848. DOI: 10.1039/C8SM02485E. URL: http://xlink.rsc.org/?DOI=C8SM02485E (visited on 10/05/2023).

[17] D. I. Dimitrov, A. Milchev, and K. Binder. “Capillary Rise in Nanopores: Molecular Dynamics Evidence for the Lucas-Washburn Equation”. In: *Physical Review Letters* 99.5 (July 31, 2007), p. 054501. ISSN: 0031-9007, 1079-7114. DOI: 10.1103/PhysRevLett.99.054501. URL: https://link.aps.org/doi/10.1103/PhysRevLett.99.054501 (visited on 10/05/2023).

[18] Hang Ding, Peter D.M. Spelt, and Chang Shu. “Diffuse Interface Model for Incompressible Two-Phase Flows with Large Density Ratios”. In: *Journal of Computational Physics* 226.2 (Oct. 2007), pp. 2078–2095. ISSN: 00219991. DOI: 10.1016/j.jcp.2007.06.028. URL: https://linkinghub.elsevier.com/retrieve/pii/S0021999107002793 (visited on 10/05/2023).

[19] Michael Dreyer, Antonio Delgado, and Hans-Joseph Path. “Capillary Rise of Liquid between Parallel Plates under Microgravity”. In: *Journal of Colloid and Interface Science* 163.1 (Mar. 1994), pp. 158–168. ISSN: 00219797. DOI: 10.1006/jcis.1994.1092. URL: https://linkinghub.elsevier.com/retrieve/pii/S0021979784710927 (visited on 10/05/2023).

[20] Mathis Fricke et al. “An Analytical Study of Capillary Rise Dynamics: Critical Conditions and Hidden Oscillations”. In: *Physica D: Nonlinear Phenomena* 455 (Dec. 2023), p. 133895. ISSN: 01672789. DOI: 10.1016/j.physd.2023.133895. arXiv: 2305.05939 [physics]. URL: http://arxiv.org/abs/2305.05939 (visited on 10/05/2023).

[21] N. Fries and M. Dreyer. “An Analytic Solution of Capillary Rise Restrained by Gravity”. In: *Journal of Colloid and Interface Science* 320.1 (Apr. 2008), pp. 259–263. ISSN: 00219797. DOI: 10.1016/j.jcis.2008.01.009. URL: https://linkinghub.elsevier.com/retrieve/pii/S0021979708000520 (visited on 10/05/2023).

[22] N. Fries and M. Dreyer. “The Transition from Inertial to Viscous Flow in Capillary Rise”. In: *Journal of Colloid and Interface Science* 327.1 (Nov. 2008), pp. 125–128. ISSN: 00219797. DOI: 10.1016/j.jcis.2008.08.018. URL: https://linkinghub.elsevier.com/retrieve/pii/S0021979708009661 (visited on 10/05/2023).

[23] Daniel Hagg. “Direkte numerische Simulation von transientem Benetzungsverhalten in komplexen Dichtspaltgeometrien unter Verwendung von phaseFieldFoam”. In: (2019). In collab. with Bettina Frohnapfel et al. DOI: 10.5445/IR/1000145948. URL: https://publikationen.bibliothek.kit.edu/1000145948 (visited on 10/05/2023).

[24] Mohammad Heiranian and Narayana R. Aluru. “Modified Lucas-Washburn Theory for Fluid Filling in Nanotubes”. In: *Physical Review E* 105.5 (May 16, 2022), p. 055105. ISSN: 2470-0045, 2470-0053. DOI: 10.1103/PhysRevE.105.055105. URL: https://link.aps.org/doi/10.1103/PhysRevE.105.055105 (visited on 10/05/2023).

[25] Michael Holzinger and TU Darmstadt. *Direct Numerical Simulation of Dynamic Droplet Wetting on Superhydrophobic Substrates by Means of a Diffuse-Interface Phase-Field Method Using OpenFOAM*. In collab. with Technical University Of Darmstadt. Technical University of Darmstadt, 2021. DOI: 10.48328/TUDATALIB-473. URL: https://tudatalib.ulb.tu-darmstadt.de/handle/tudatalib/2689 (visited on 10/05/2023).

[26] Chun Huh and L.E Scriven. "Hydrodynamic Model of Steady Movement of a Solid/Liquid/Fluid Contact Line". In: *Journal of Colloid and Interface Science* 35.1 (Jan. 1971), pp. 85–101. ISSN: 00219797. DOI: 10.1016/0021-9797(71)90188-3. URL: https://linkinghub.elsevier.com/retrieve/pii/0021979771901883 (visited on 10/05/2023).

[27] David Jacqmin. "Calculation of Two-Phase Navier–Stokes Flows Using Phase-Field Modeling". In: *Journal of Computational Physics* 155.1 (Oct. 1999), pp. 96–127. ISSN: 00219991. DOI: 10.1006/jcph.1999.6332. URL: https://linkinghub.elsevier.com/retrieve/pii/S0021999199963325 (visited on 10/05/2023).

[28] David Jacqmin. "Contact-Line Dynamics of a Diffuse Fluid Interface". In: *Journal of Fluid Mechanics* 402 (Jan. 10, 2000), pp. 57–88. ISSN: 0022-1120, 1469-7645. DOI: 10.1017/S0022112099006874. URL: https://www.cambridge.org/core/product/identifier/S0022112099006874/type/journal_article (visited on 10/05/2023).

[29] F. Jamshidi et al. "On Suitability of Phase-Field and Algebraic Volume-of-Fluid OpenFOAM® Solvers for Gas–Liquid Microfluidic Applications". In: *Computer Physics Communications* 236 (Mar. 2019), pp. 72–85. ISSN: 00104655. DOI: 10.1016/j.cpc.2018.10.015. URL: https://linkinghub.elsevier.com/retrieve/pii/S0010465518303631 (visited on 10/05/2023).

[30] Cahn John W. and Hillard John E. "Free Energy of a Nonuniform System. I. Interfacial Free Energy". In: 28.2 (Feb. 1958). DOI: 10.1063/1.1744102.

[31] Uğis Lācis et al. "Nanoscale Sheared Droplet: Volume-of-Fluid, Phase-Field and No-Slip Molecular Dynamics". In: *Journal of Fluid Mechanics* 940 (June 10, 2022), A10. ISSN: 0022-1120, 1469-7645. DOI: 10.1017/jfm.2022.219. URL: https://www.cambridge.org/core/product/identifier/S0022112022002191/type/journal_article (visited on 10/09/2023).

[32] Richard Lucas. "Ueber das Zeitgesetz des kapillaren Aufstiegs von Flüssigkeiten". In: *Kolloid-Zeitschrift* 23.1 (July 1918), pp. 15–22. ISSN: 0303-402X, 1435-1536. DOI: 10.1007/BF01461107. URL: http://link.springer.com/10.1007/BF01461107 (visited on 10/05/2023).

[33] G. Martic et al. "A Molecular Dynamics Simulation of Capillary Imbibition". In: *Langmuir* 18.21 (Oct. 1, 2002), pp. 7971–7976. ISSN: 0743-7463, 1520-5827. DOI: 10.1021/la020068n. URL: https://pubs.acs.org/doi/10.1021/la020068n (visited on 10/05/2023).

[34] Alireza Mohammad Karim. “A Review of Physics of Moving Contact Line Dynamics Models and Its Applications in Interfacial Science”. In: *Journal of Applied Physics* 132.8 (Aug. 28, 2022), p. 080701. ISSN: 0021-8979, 1089-7550. DOI: 10.1063/5.0102028. URL: https://pubs.aip.org/jap/article/132/8/080701/2837259/A-review-of-physics-of-moving-contact-line (visited on 10/05/2023).

[35] Tiezheng Qian, Xiao-Ping Wang, and Ping Sheng. “A Variational Approach to Moving Contact Line Hydrodynamics”. In: *Journal of Fluid Mechanics* 564 (Oct. 2006), p. 333. ISSN: 0022-1120, 1469-7645. DOI: 10.1017/S0022112006001935. URL: http://www.journals.cambridge.org/abstract_S0022112006001935 (visited on 10/05/2023).

[36] D Quéré. “Inertial Capillarity”. In: *Europhysics Letters (EPL)* 39.5 (Sept. 1, 1997), pp. 533–538. ISSN: 0295-5075, 1286-4854. DOI: 10.1209/epl/i1997-00389-2. URL: https://iopscience.iop.org/article/10.1209/epl/i1997-00389-2 (visited on 10/05/2023).

[37] Élfego Ruiz-Gutiérrez et al. “The Long Cross-over Dynamics of Capillary Imbibition”. In: *Journal of Fluid Mechanics* 939 (May 25, 2022), A39. ISSN: 0022-1120, 1469-7645. DOI: 10.1017/jfm.2022.248. URL: https://www.cambridge.org/core/product/identifier/S0022112022002488/type/journal_article (visited on 10/05/2023).

[38] N. Samkhaniani et al. “Bouncing Drop Impingement on Heated Hydrophobic Surfaces”. In: *International Journal of Heat and Mass Transfer* 180 (Dec. 2021), p. 121777. ISSN: 00179310. DOI: 10.1016/j.ijheatmasstransfer.2021.121777. URL: https://linkinghub.elsevier.com/retrieve/pii/S0017931021008826 (visited on 10/05/2023).

[39] Robert Siegel. “Transient Capillary Rise in Reduced and Zero-Gravity Fields”. In: *Journal of Applied Mechanics* 28.2 (June 1, 1961), pp. 165–170. ISSN: 0021-8936, 1528-9036. DOI: 10.1115/1.3641647. URL: https://asmedigitalcollection.asme.org/appliedmechanics/article/28/2/165/385908/Transient-Capillary-Rise-in-Reduced-and (visited on 10/05/2023).

[40] Michael Stange, Michael E. Dreyer, and Hans J. Rath. “Capillary Driven Flow in Circular Cylindrical Tubes”. In: *Physics of Fluids* 15.9 (Sept. 1, 2003), pp. 2587–2601. ISSN: 1070-6631, 1089-7666. DOI: 10.1063/1.1596913. URL: https://pubs.aip.org/pof/article/15/9/2587/450889/Capillary-driven-flow-in-circular-cylindrical (visited on 10/05/2023).

[41] J. D. Van Der Waals. “The Thermodynamic Theory of Capillarity under the Hypothesis of a Continuous Variation of Density”. In: *Journal of Statistical Physics* 20.2 (Feb. 1979), pp. 200–244. ISSN: 0022-4715, 1572-9613. DOI: 10.1007/BF01011514. URL: http://link.springer.com/10.1007/BF01011514 (visited on 10/05/2023).

[42] O. V. Voinov. “Hydrodynamics of Wetting”. In: *Fluid Dynamics* 11.5 (1977), pp. 714–721. ISSN: 0015-4628, 1573-8507. DOI: 10.1007/BF01012963. URL: http://link.springer.com/10.1007/BF01012963 (visited on 10/05/2023).

[43] Edward W. Washburn. “The Dynamics of Capillary Flow”. In: *Physical Review* 17.3 (Mar. 1, 1921), pp. 273–283. ISSN: 0031-899X. DOI: 10.1103/PhysRev.17.273. URL: https://link.aps.org/doi/10.1103/PhysRev.17.273 (visited on 10/05/2023).

[44] Martin Wörner et al. “Spreading and Rebound Dynamics of Sub-Millimetre Urea-Water-Solution Droplets Impinging on Substrates of Varying Wettability”. In: *Applied Mathematical Modelling* 95 (July 2021), pp. 53–73. ISSN: 0307904X. DOI: 10.1016/j.apm.2021.01.038. URL: https://linkinghub.elsevier.com/retrieve/pii/S0307904X2100055X (visited on 10/05/2023).

[45] Pingkeng Wu, Alex D. Nikolov, and Darsh T. Wasan. “Capillary Rise: Validity of the Dynamic Contact Angle Models”. In: *Langmuir* 33.32 (Aug. 15, 2017), pp. 7862–7872. ISSN: 0743-7463, 1520-5827. DOI: 10.1021/acs.langmuir.7b01762. URL: https://pubs.acs.org/doi/10.1021/acs.langmuir.7b01762 (visited on 10/05/2023).

[46] Mariana Ye Yin. “Direct Numerical Simulation of Droplets Moving on an Inclined Surface by a Diffuse-Interface Phase-Field Method Using OpenFOAM”. In: ().

[47] Thomas Young. “III. An Essay on the Cohesion of Fluids”. In: *Philosophical Transactions of the Royal Society of London* 95 (Dec. 31, 1805), pp. 65–87. ISSN: 0261-0523, 2053-9223. DOI: 10.1098/rstl.1805.0005. URL: https://royalsocietypublishing.org/doi/10.1098/rstl.1805.0005 (visited on 10/12/2023).

[48] P. Yue and J. J. Feng. “Can Diffuse-Interface Models Quantitatively Describe Moving Contact Lines?” In: *The European Physical Journal Special Topics* 197.1 (Aug. 2011), pp. 37–46. ISSN: 1951-6355, 1951-6401. DOI: 10.1140/epjst/e2011-01434-y. URL: http://link.springer.com/10.1140/epjst/e2011-01434-y (visited on 10/05/2023).

[49] Pengtao Yue and James J. Feng. “Wall Energy Relaxation in the Cahn–Hilliard Model for Moving Contact Lines”. In: *Physics of Fluids* 23.1 (Jan. 1, 2011), p. 012106. ISSN: 1070-6631, 1089-7666. DOI: 10.1063/1.3541806. URL: https://pubs.aip.org/pof/article/23/1/012106/937545/Wall-energy-relaxation-in-the-Cahn-Hilliard-model (visited on 10/05/2023).

[50] Pengtao Yue, Chunfeng Zhou, and James J. Feng. “Sharp-Interface Limit of the Cahn–Hilliard Model for Moving Contact Lines”. In: *Journal of Fluid Mechanics* 645 (Feb. 25, 2010), pp. 279–294. ISSN: 0022-1120, 1469-7645. DOI: 10.1017/S0022112009992679. URL: https://www.cambridge.org/core/product/identifier/S0022112009992679/type/journal_article (visited on 10/05/2023).

[51] B.V. Zhmud, F. Tiberg, and K. Hallstensson. “Dynamics of Capillary Rise”. In: *Journal of Colloid and Interface Science* 228.2 (Aug. 2000), pp. 263–269. ISSN: 00219797. DOI: 10.1006/jcis.2000.6951. URL: https://linkinghub.elsevier.com/retrieve/pii/S0021979700969510 (visited on 10/05/2023).